Turning Flight Simulation with Fluid-rigid Body Interaction for Flying Car with Contra-rotating Propellers

A. Takii[1,2], R. Gomi[2], M. Yamakawa[2] and M. Tsubokura[1,3]

[1] RIKEN Center for Computational Science, 7-1-26 Minatojima-minami-machi, Chuo-ku, Kobe, Hyogo 650-0047, Japan
[2] Kyoto Institute of Technology, Matsugasaki, Sakyo-ku, Kyoto 606-8585, Japan
[3] Graduate School of System Informatics, Kobe University 1-1 Rokkodai, Nada-ku, Kobe, Hyogo 657-8501, Japan
ayato.takii@riken.jp

Abstract. Toward realization of the Digital Flight for the next-generation vehicle, numerical simulation of turning flights of a flying car was performed with consideration of fluid-rigid body interaction. The vehicle use in the paper is electric vertical takeoff and landing (eVTOL) octorotor type with four contra-rotating propeller units which successfully performed manned flight test. The simulation is conducted such that the flying car mimicks its real-world counterpart by generating force solely through the rotation of its eight propellers. The moving computational domain method was adopted to realize the free movement of the vehicle in three-dimensional space. The whole computational grid is divided into eight domains to reproduce rotation of propellers. The propeller rotations are achieved without any simplification by applying the multi-axis sliding mesh approach. Moreover, to fly the flying car as intended, an attitude of the body in the flight is controlled properly to by the proportional-integral-derivative（PID) controller. As a result, the vehicle flies under only the lift generated by the propeller and the turning flights of a flying car with coaxial propellers are reproduced. In addition, this simulation results are different from analytical results based on simplified aerodynamic force. Therefore, it is suggested that this method is the effective one for numerical flight tests of a multi-rotor aircraft on a computer.

Keywords: CFD, Coupled Simulation, Moving Boundary.

1 Introduction

Currently, there is an urgent necessity to reach net-zero carbon emissions to prevent environmental issues. Most countries are planning to achieve that by 2050-2070, and a promising movement for carbon neutrality is taking shape in the world [1]. One of strategies to reach a carbon neutrality is the streamlining and the electrification of the transportation. In recent years, small unmanned aerial vehicles called drones have become popular. As the next stage, the realization of aircrafts that can be easily used

ICCS Camera Ready Version 2023
To cite this paper please use the final published version:
DOI: 10.1007/978-3-031-35995-8_40

by individuals is expected, and these are expected as countermeasures against environmental problems and urban traffic problems. It's also reported that those flying cars have less greenhouse gas emissions than gasoline vehicles for long-distance transportation [2]. The different type of flying cars, especially electric vertical takeoff and landing (eVTOL) vehicles, are being developed around the world as next-generation mobility [3]. Practical use of eVTOL vehicles, as the new type of mobility, requires numerous tests to confirm safety, and cost a great deal of development time. Until now, aircraft development sites have adopted a method of repeating prototyping and testing, which has resulted in enormous amounts of time and money being spent. For eVTOL aerodynamic performance evaluation, various studies have been conducted. Experimental studies of eVTOL aircraft conducted to measure lift and drag forces through wind tunnel test [4] and to visualize the flow field around rotating rotors using particle image velocimetry [5]. Numerical simulations were employed to study the aerodynamic interaction of coaxial propellers [6]. The simulations considering the entire aircraft were done by modeling propeller lift [7] or by computing actual propeller rotation [8]. However, these studies were in the way of numerical wind tunnel with fixed body in Euler coordinate system and mainly focused on steady state. This means that most of previous studies focuses only on a few aspects of eVTOL aerodynamic performance. To design a safe airframe as intended, it is necessary to analyze the behavior of the airframe more comprehensively and practically.

The aim of realistic numerical flight simulation is to achieve Digital Flight [9], which facilitates the simulation and analysis of various types of flights using only computers, including take-off, landing, and emergency scenarios. This approach simplifies the analysis of the high-risk flight conditions and enables the execution of large-scale experiments that are difficult to carry out physically and socially. Consequently, Digital Flight leads to safer airframe designs at a lower cost. Currently, although the progress of computers' development doesn't catch up with the realization of complete Digital Flight, we have conducted some realistic flight simulations considering fluid-aircraft interaction [10,11]. In present work, this method is newly applied to the eVTOL flying car. Few reports are available on the numerical flight simulation of eVTOL flying. The numerical simulation has a difficulty with a dynamically moving grid as well as complexity of feedback control for multi-rotor. Numerical simulation of turning flights of aircraft is challenging due to the complex attitude variation, acceleration, and long-distance travel involved. Although turning flight is frequently used in practice, it remains difficult to simulate. This study overcomes these challenges by applying Digital Flight to an eVTOL flying car, and performing a turning flight simulation.

As the model of the eVTOL flying car, we adopt an octorotor type with four contra-rotating propeller units which successfully performed manned flight test. This type is one of the choices for practical use due to the compactness of the body and the safety to keep the vehicle maneuverable in the event of propeller trouble, which is attributed to propeller redundancy. To reproduce realistic flight, the coupled computation between airflow and flying car is performed regarding the eVTOL flying car as a rigid body; that is, the airflow is driven by rotations of propellers, and the flying car flies only by the fluid forces applied to that body. Unsteady motion of the flying car is

ICCS Camera Ready Version 2023
To cite this paper please use the final published version:
DOI: 10.1007/978-3-031-35995-8_40

complex moving boundary problem in computational fluid dynamics. Although there are some approaches for solving moving boundary problem such as the arbitrary Lagrangian-Eulerian (ALE) [13,14] and the immersed boundary method (IBM) [15, 16], we adopt the moving-grid finite-volume method (MGFV) method [17] which satisfies the geometric conservation law (GCL) automatically and derives the accurate fluid force with unstructured body fitted grid. The MGFV method allows deformation of the computational grid points by discretizing the governing equations in the space-time unified four-dimensional control volume. In addition, we use the moving computational domain (MCD) method [18] to enable a flying car to navigate a wide range of space compared with its own size. In this method, the whole computational grid moves accordingly to the motion of the object so that the flight of the flying car is not constrained by the size of the computational grid. Futhermore, we directly compute propeller rotations by combining with the multi-axis sliding mesh approach [19]. To fly the car as intended, the eight propellers must be controlled properly so that the attitude is stable. The proportional-integral-derivative control is used as the feedback system. This study demonstrates numerical flight simulation considering fluid-rigid body interactions for eVTOL flying car with contra-rotating propellers.

2 Numerical Approach

2.1 Governing Equations

In this study, a flying car flies a long distance consuming a tremendous wall-clock time to complete the numerical simulation. Therefore, this research uses the Euler equation as governing equation of compressible flow to reduce the computation time after considering that this simulation has high Reynolds number and low influence of viscosity. The flow equations and ideal gas law are given as follows:

$$\frac{\partial \boldsymbol{q}}{\partial t}+\frac{\partial \boldsymbol{E}}{\partial x}+\frac{\partial \boldsymbol{F}}{\partial y}+\frac{\partial \boldsymbol{G}}{\partial z}=0, \tag{1}$$

$$\boldsymbol{q}=\begin{bmatrix}\rho\\ \rho u\\ \rho v\\ \rho w\\ e\end{bmatrix}, \boldsymbol{E}=\begin{bmatrix}\rho u\\ \rho u^2+p\\ \rho uv\\ \rho uw\\ u(e+p)\end{bmatrix}, \boldsymbol{F}=\begin{bmatrix}\rho v\\ \rho uv\\ \rho v^2+p\\ \rho vw\\ v(e+p)\end{bmatrix}, \boldsymbol{G}=\begin{bmatrix}\rho w\\ \rho uw\\ \rho vw\\ \rho w^2+p\\ w(e+p)\end{bmatrix}, \tag{2}$$

$$p=(\gamma-1)\left[e-\frac{1}{2}\rho(u^2+v^2+w^2)\right], \tag{3}$$

where $\boldsymbol{q}$ is the vector of conserved variables, $\boldsymbol{E}$, $\boldsymbol{F}$ and $\boldsymbol{G}$ are the convective flux vectors, ρ is the density, u,v and w are the corresponding velocity components in the x, y and z-directions, respectively, p is the pressure and e is the total energy per unit volume. The ratio of specific heats γ is 1.4 in this study. Each variable is nondimensionalized as follows:

$$\begin{gathered}x=\frac{\tilde{x}}{\tilde{L}},\ y=\frac{\tilde{y}}{\tilde{L}},\ z=\frac{\tilde{z}}{\tilde{L}},\ t=\frac{\tilde{t}}{\tilde{L}/\tilde{U}},\\ \tilde{p}=\frac{\tilde{p}}{\tilde{\rho}\tilde{U}^2},\ u=\frac{\tilde{u}}{\tilde{U}},\ v=\frac{\tilde{v}}{\tilde{U}},\ w=\frac{\tilde{w}}{\tilde{U}}.\end{gathered} \tag{4}$$

ICCS Camera Ready Version 2023
To cite this paper please use the final published version:
DOI: 10.1007/978-3-031-35995-8_40

Where (~) represents a dimensional quantity; $\tilde{L}$ (4 m) is the characteristic length, $\tilde{U}$ (340 m/s) is the characteristic velocity, $\tilde{\rho}$ (1.2 kg/m^3) is the density of the air.

The computational grid utilizes the body-fitted unstructured mesh with collocated arrangement; the values of the physical parameters are defined at cell centers. The governing equations are discretized by the MGFV method. This is a dynamic mesh method which is automatically satisfied by discretization performed using a four-dimensional control volume in the space and time unified domain, which enables deformation of the computational grid points. The convective flux vectors on faces of the control volume are evaluated by the Roe flux difference splitting scheme [20]. The conserved variables in the cell are reconstructed by the monotonic upstream-centered scheme for conservation laws (MUSCL) approach with Hishida's van Leer-like limiter [21]. To solve discretized equations, the dual time stepping is adopted. The two-stage Runge-Kutta method [22] is used for the pseudo time marching.

2.2 Moving computational domain approach

The flying car moves in much wider space than its computational grid size. In conventional approach using a fixed computational domain, the flying car can't travel infinite distance due to the grid size limitation. To deal with such simulation, we use the moving computational domain approach based on the MGFV method. In this MCD method, the whole computational domain including a body inside moves rigidly in the world space (see Fig. 1). Thus, there is no limitation of the flight distance. The rotation of the propellers was achieved through a combination of the multi-axis sliding mesh approach [23] and the approach of moving the entire computational domain.

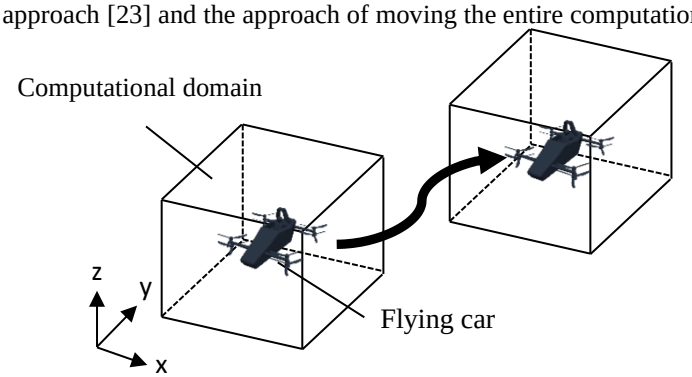

Fig. 1. Conceptual diagram of the moving computational domain method. The whole computational domain including a body inside moves rigidly in the world space.

2.3 Coupled Simulation with Rigid Body

In this study, the flight simulation of the flying car is conducted with fluid-rigid body interaction. A fluid flow around the flying car is driven by rotating propellers of that; the attitude and position of the car are determined by the fluid force of the air. The

ICCS Camera Ready Version 2023
To cite this paper please use the final published version:
DOI: 10.1007/978-3-031-35995-8_40

rigid body motion is determined by the Newton's equation of motion and the Euler's as follows:

$$m\frac{d^2\boldsymbol{r}}{dt^2} = \boldsymbol{F}, \tag{5}$$

$$I\frac{d\boldsymbol{\omega}}{dt} + \boldsymbol{\omega} \times I\boldsymbol{\omega} = \boldsymbol{T}, \tag{6}$$

where m is the mass, $\boldsymbol{r}$ is the position, $\boldsymbol{F}$ is the force, I is the inertia tensor, $\boldsymbol{\omega}$ is the angular velocity and $\boldsymbol{T}$ is the torque. The force and torque applying to the flying car are calculated by integrating the pressure of the flow fluid on surface of the body. This simulation is weak coupling where the translation and rotation of the flying car are performed once every time step by using the force and the torque from the previous time step.

3 Flight Simulation of eVTOL Flying Car

3.1 Computational Model

The model of a flying car is based on SD-03, which was developed by SkyDrive in Japan [12]. The model has totally 8 propellers in total consisting of four contra-rotating propeller units. The flying car's mass is 400 kg, the overall length of the vehicle $\tilde{L}$, which is used as the characteristic length, is 4 m. The inertia tensor to solve the motion equations is calculated by integrating in the volume domain assuming that the density is uniform. The computational grid was created by MEGG3D [24,25] shown as Fig. 2. The shape of the grid is a sphere with diameter of $30\tilde{L}$ and total number of grid cells is ~3,000,000. The whole grid consists of several domains, i.e. eight propeller domains and the fuselage domain, to reproduce motions of each component by using the multi-axis sliding mesh approach (see Fig. 3).

The initial values of flow fields are as follows: $\rho = 1.0$, $p = 1.0/\gamma$, $(u,v,w) = (0,0,0)$. The boundary conditions are as follows: the slip condition for body of the flying car, the Riemann boundary condition for outer of the computational grid.

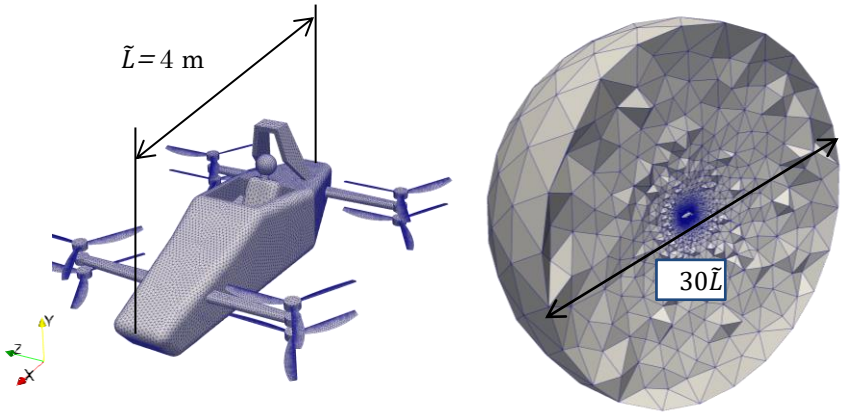

Fig. 2. Surface mesh of the flying car and the computational grid.

ICCS Camera Ready Version 2023
To cite this paper please use the final published version:
DOI: 10.1007/978-3-031-35995-8_40

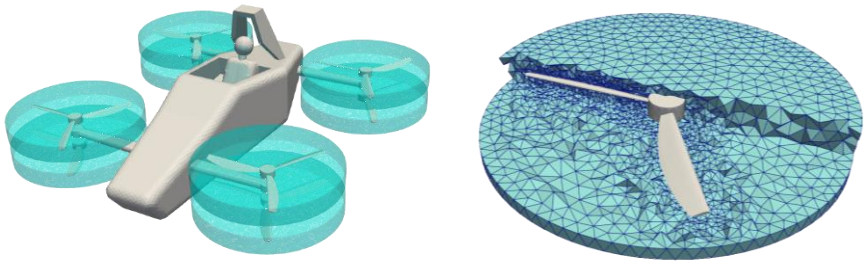

Fig. 3. Domain division for the sliding mesh approach and grid of a propeller domain.

3.2 Control model

The flying car is subject to forces from the surrounding airflow and moves freely in space. To fly the vehicle as intended, the eight propellers must be controlled properly so that the attitude is stable. We use the PID control as feedback system. The rotation of the propellers is determined by the superposition of four operation variables: the throttle to control the altitude, the aileron to control the roll, the rudder to control the yaw, and the elevator to control the pitch. To get the target attitude, the operating value of the rotation of the propellers $h(t)$ is determined by the following equations:

$$h(t) = K_{\mathrm{p}} e(t) + K_{\mathrm{i}} \int_0^t e(\tau)\mathrm{d}\tau + \frac{K_{\mathrm{d}} \mathrm{d}e(t)}{\mathrm{d}t}, \tag{7}$$

$$e(t) = r_{\mathrm{target}}(t) - r_{\mathrm{current}}(t), \tag{8}$$

where $e(t)$ is the error, $r_{\mathrm{target}}(t)$ is the target value and $r_{\mathrm{current}}(t)$ is the current value. K_{p}, K_{i} and K_{d} are the proportional, integral and differential gain. These gains are determined by tuning the linear single-input single-output (SISO) transfer function model while checking their step responses. Here, the kinematic model of the flying car is linearized by assuming that the changes in the propeller speed are enough small in the equations of the motion. By applying the mixing process [26], this model can be considered as a SISO system without coupling for target values. The transfer functions in the Laplace domain are regarded as follows:

$$\frac{\omega_{\mathrm{roll}}(s)}{h_{\mathrm{roll}}} = \frac{DK_T}{I_{xx}s}, \tag{9}$$

$$\frac{\omega_{\mathrm{pitch}}(s)}{h_{\mathrm{pitch}}} = \frac{LK_T}{I_{zz}s}, \tag{10}$$

$$\frac{\omega_{\mathrm{yaw}}(\mathrm{s})}{h_{\mathrm{yaw}}} = \frac{K_A}{I_{yy}s}, \tag{11}$$

ICCS Camera Ready Version 2023
To cite this paper please use the final published version:
DOI: 10.1007/978-3-031-35995-8_40

$$\frac{v_y(s)}{h_{\text{throttle}}} = -\frac{K_T}{ms}, \tag{12}$$

where h_{roll}, h_{pitch}, h_{yaw} are the control inputs for aircraft principal axes and $h_{throttle}$ is input for thrust. $\omega_{\text{roll}}, \omega_{\text{pitch}}$ and ω_{yaw} are the angular velocities in the direction of roll, pitch and yaw axes. I is the inertia tensor, v_y is the velocity in vertical direction, D is the distance from the center of the flying car to the propeller axis of rotation. d K_T and K_A are coefficients obtained from the lift and torque of a propeller [27].

3.3 Flight Condition

In present work, the flying car flies as follows.

1. Set the target forward velocity to 60 km/h and start accelerating. Here, the absolute value of the target pitch angle is limited within 15 degrees.

2. After the difference between the target speed and the current speed fell below 2 km/h, the target roll angle is set to 30 degrees to start the turning flight.

3. After the aircraft turns 90 degrees, stop turning flight and let the aircraft go straight.

The gains for each controlled values are shown in Table 1, where v_{x} is forward velocity, θ_{roll}, θ_{pitch} and θ_{yaw} are the angles of roll, pitch, yaw of the flying car.

Table 1. Control gain in turning flight of the flying car.

Input	v_y	ω_{roll}	ω_{pitch}	ω_{yaw}
Output	h_{throttle}	h_{roll}	h_{pitch}	h_{yaw}
K_{p}	2×10^4	3×10^2	2×10^3	5×10^3
K_{i}	2×10^{-1}	3×10^{-3}	2×10^{-2}	5×10^{-2}
K_{d}	1×10^4	1×10^2	8×10^2	8×10^3

Input	y	v_x	θ_{roll}	θ_{pitch}	θ_{yaw}
Output	v_y	θ_{pitch}	ω_{roll}	ω_{pitch}	ω_{yaw}
K_{p}	4.5×10^3	2×10^3	7.4	7.4	1.5
K_{i}	0	1×10^1	0	0	0
K_{d}	0	2×10^4	0	0	0

ICCS Camera Ready Version 2023
To cite this paper please use the final published version:
DOI: 10.1007/978-3-031-35995-8_40

4 Result and Discussion

As the result of coupling simulation between fluid and rigid body with the PID control, the flying car flied stably with turning around. The trajectory of turning flight at 60 km/h is shown in Fig. 4. The size of square grid of the figure is 10 m. The car flied ~140 m in the x-direction from start of acceleration to finishing of 90 degrees turning flight. This cruising distance is more than double size of the computational grid. Next, the time variations of flight attitude and forward velocity are shown in Fig. 5 (a). The dotted line in the figure indicates the target forward velocity of 60 km/h. After the current velocity approached to the target velocity at 9 s, the velocity of the car is adjusted by increasing or decreasing its pitch angle. In the turning, the roll angle almost fitted the target value 30 degrees although an overshoot occurred at the end of the turn. The time variations of the handling values for maneuvering attitude and the altitude of the flying car are shown in Fig. 5 (b). The handling values changed rapidly at the start and end of turning. At time is 14s, the flying car failed to keep constant altitude under the influence of a huge rudder input occurred at the end of the turn.

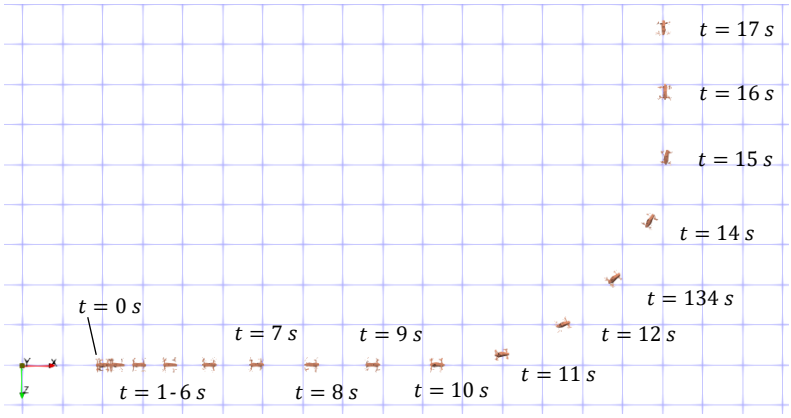

Fig. 4. The trajectory of the flying car in turning flight at 60 km/h.

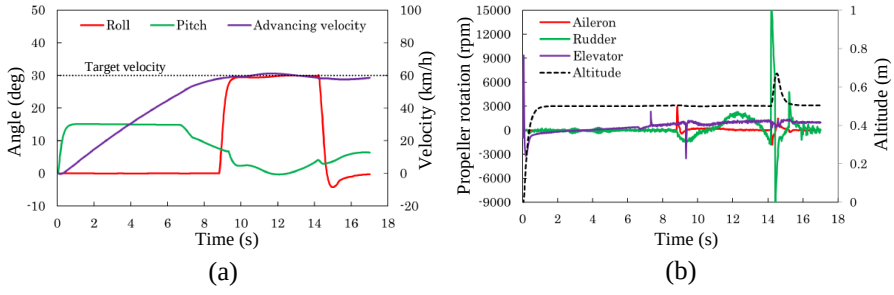

Fig. 5. Time variations of (a) attitude and forward velocity, and (b) handling values for maneuvering the attitude and altitude of the flying car.

ICCS Camera Ready Version 2023
To cite this paper please use the final published version:
DOI: 10.1007/978-3-031-35995-8_40

Next, this result is compared with a simple theoretical solution. Assuming that the flight altitude and forward velocity are constant, the theoretical turning radius is calculated as follows:

$$r = \frac{v^2}{g\tan\theta}, \tag{13}$$

where v is the forward velocity of the car, g is the gravitational acceleration and θ is the roll angle. By this equation, the theoretical turning radius with the forward velocity of 60 km/h and the roll angle of 30 degrees is 49.0 m. The turning radius in the numerical simulation is calculated by fitting the trajectory data to the circle equation with the least squares method. Used trajectory is the section of 30 degrees roll angle in the x-z plane. A circle of the obtained radius and the trajectory of the flying car are shown in Fig. 6. The turning radius obtained by fitting is 59.8 m. This is 22% larger than the theoretical turning radius. This may be affected by non-constant centripetal force (~10% fluctuation) during turning, as shown in Fig. 6 (b). This result clarified that numerical simulation considering the aerodynamics is necessary to predict the turning motion of the flying car accurately.

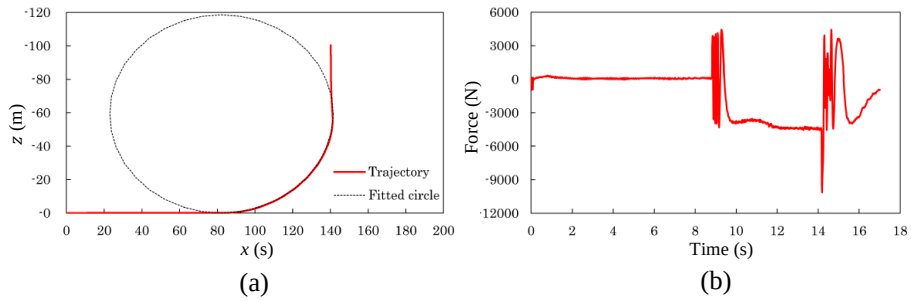

Fig. 6. (a) trajectory of the flying car and fitted circle. (b) Time variation of centripetal force.

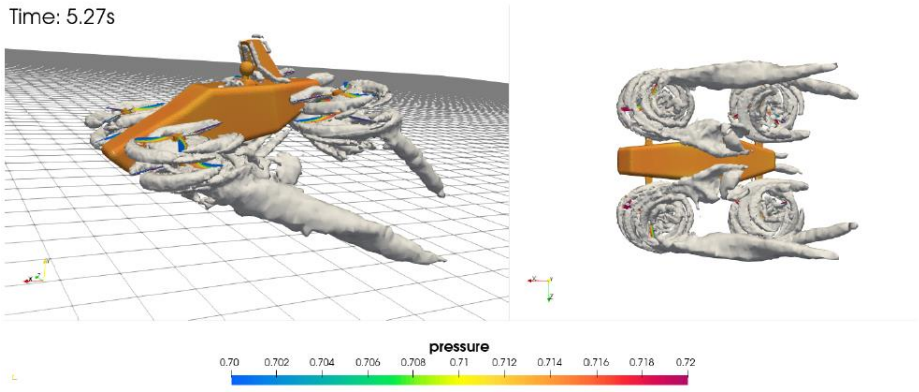

Fig. 7. Pressure contour on the flying car and isosurface of Q-criterion (Q=0.1) during acceleration.

ICCS Camera Ready Version 2023
To cite this paper please use the final published version:
DOI: 10.1007/978-3-031-35995-8_40

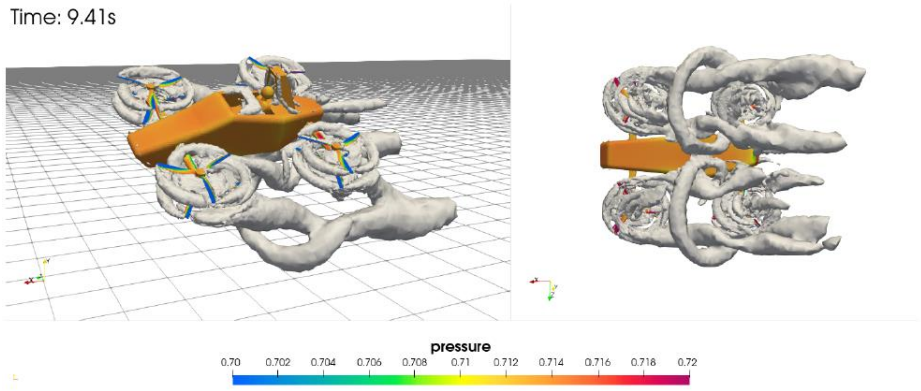

Fig. 8. Pressure contour on the flying car and isosurface of Q-criterion (Q=0.1) at start of turning

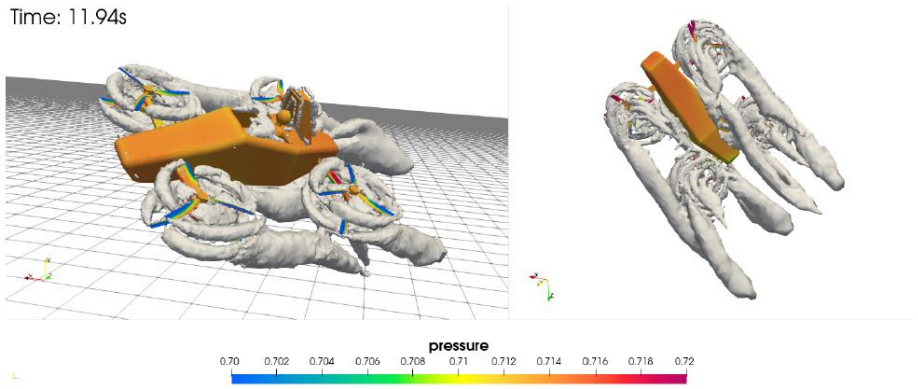

Fig. 9. Pressure contour on the flying car and isosurface of Q-criterion (Q=0.1) during turning.

Figure 7-9 show pressure contour on the flying car and isosurface of Q-criterion (Q=0.1) of the flow field around the body: during acceleration, at the start of the turn and during turning, respectively. The left is the perspective view, and the right is the bottom view of the body. In every flight stage, the complex vortices are generated by multiple propellers. While turning, the vortices from the front propellers are dragged backward and reach rear propellers. The vortex shape is more complicated at the transition stage of motion. This numerical simulation revealed such unsteadiness in turning flight.

5 Conclusions

Turning flight simulation was computed for the eVTOL flying car with contra-rotating, considering the fluid and rigid body interaction. The MCD method based on the unstructured MGFV method was used to enable the flying car to move in the infi-

ICCS Camera Ready Version 2023
To cite this paper please use the final published version:
DOI: 10.1007/978-3-031-35995-8_40

nite world space without limitation of its computational size. Moreover, the multi-axis sliding mesh approach was adopted to rotate eight propellers of the flying car. To fly the flying car as intended, the PID controller is used to control the number of rotations of eight propellers so that the flight attitude such as pitch, roll and yaw were controlled properly. As a result of the coupled computation between the flow field and the rigid body using above approach, the flying car obtained the lift by rotating its propellers and flew in turning. Next, the flight trajectory was compared with the theoretical turning radius. The turning radius obtained from this numerical simulation was 22% larger than the theoretical one, which implies numerical simulation considering aerodynamics is important to predict the flight of the flying car. Finally, this realistic flight simulation allowed for the visualization of complex flow fields around the flying car and has the potential to provide valuable information for the future development of such vehicles, which would be difficult to obtain through experiments and conventional stational simulations.

Acknowledgments

This paper is based on results obtained from a project, JPNP14004, subsidized by the New Energy and Industrial Technology Development Organization (NEDO).

References

1. Chen, L., Msigwa, G., Yang, M., Osman, A. I., Fawzy, S., Rooney, D. W., Yap, P. S.; Strategies to achieve a carbon neutral society: a review. Environmental Chemistry Letters, 20(4), 2277-2310 (2022).
2. Kasliwal, A., et al.: Role of flying cars in sustainable mobility. Nature communications, 10(1), 1555 (2019).
3. Bacchini, A., Cestino, E.: Electric VTOL configurations comparison. Aerospace, 6(3), 26 (2019).
4. Pardede, W. M., Adhitya, M.: Take off and landing performance analysis for a flying car model using wind tunnel test method. In AIP Conference Proceedings, Vol. 2227, No. 1, p. 020030 AIP Publishing LLC (2020).
5. Zanotti, A.: Experimental study of the aerodynamic interaction between side-by-side propellers in evtol airplane mode through stereoscopic particle image velocimetry. Aerospace, 8(9), 239 (2021).
6. Cornelius, J. K., Schmitz, S., Kinzel, M. P.: Efficient computational fluid dynamics approach for coaxial rotor simulations in hover. Journal of aircraft, 58(1), 197-202 (2021).
7. Alvarez, E. J., Ning, A.: High-fidelity modeling of multirotor aerodynamic interactions for aircraft design. AIAA Journal, 58(10), 4385-4400 (2020).
8. Zhu, H., Nie, H., Zhang, L., Wei, X., Zhang, M.: Design and assessment of octocopter drones with improved aerodynamic efficiency and performance. Aerospace Science and Technology, 106, 106206 (2020).
9. M.D. Salas.: Digital Flight: The Last CFD Aeronautical Grand Challenge, Journal of Scientific Computing 28 (2-3), 479-505 (2006)
10. Takii, A., Yamakawa, M., Asao, S., Tajiri, K.: Six degrees of freedom numerical simulation of tilt-rotor plane. Lecture Notes in Computer Science, vol 11536, 506-519 (2019).

ICCS Camera Ready Version 2023
To cite this paper please use the final published version:
DOI: 10.1007/978-3-031-35995-8_40

11. Takii, A., Yamakawa, M., Asao, S.: Descending Flight Simulation of Tiltrotor Aircraft at Different Descent Rates. Lecture Notes in Computer Science, vol 12143, 178-190 (2020)
12. SkyDrive Inc (2022) Homepage. https://en.skydrive2020.com/. Accessed 1 February 2023
13. Belytschko T.: Fluid-structure interaction. Comput Struct, 12(4), 459–469 (1980).
14. Hu, H. H., Patankar, N. A., Zhu, M.: Direct numerical simulations of fluid–solid systems using the arbitrary Lagrangian–Eulerian technique. Journal of Computational Physics, 169(2), 427-462 (2001).
15. Peskin, C. S.: Flow patterns around heart valves: a numerical method. Journal of computational physics, 10(2), 252-271 (1972).
16. Peskin, C. S.: The immersed boundary method. Acta numerica, 11, 479-517 (2002).
17. Matsuno, K., Mihara, K., Satofuka, N.: A moving-mesh finite-volume scheme for compressible flows. In Computational Fluid Dynamics 2000: Proceedings of the First International Conference on Computational Fluid Dynamics, pp.705-710. Springer Berlin Heidelberg, Kyoto, Japan (2000)
18. Watanabe, K., Matsuno, K.: Moving computational domain method and its application to flow around a high-speed car passing through a hairpin curve. Journal of computational Science and Technology, 3(2), 449-459 (2009).
19. Takii, A., Yamakawa, M., Asao, S., Tajiri, K.: Six degrees of freedom flight simulation of tilt-rotor aircraft with nacelle conversion. Journal of Computational Science, 44, 101164 (2020).
20. Roe, P. L.: Approximate Riemann solvers, parameter vectors, and difference schemes. Journal of computational physics, 43(2), 357-372 (1981).
21. Hishida, M., Hashimoto, A., Murakami, K., Aoyama, T.: A new slope limiter for fast unstructured CFD solver FaSTAR. In Proceedings of 42nd Fluid Dynamics Conference/Aerospace Numerical Simulation Symposium, pp. 1-10 (2010).
22. A. Wambecq.: Rational Runge-Kutta methods for solving systems of ordinary differential equations, Computing, 20-4, 333–342 (1978)
23. Takii, A., Yamakawa, M., Asao, S., Tajiri, K.: Six degrees of freedom flight simulation of tilt-rotor aircraft with nacelle conversion. Journal of Computational Science, 44, 101164 (2020).
24. Ito, Y., Nakahashi, K.: Surface triangulation for polygonal models based on CAD data. International Journal for Numerical Methods in Fluids, 39(1), 75-96 (2002).
25. Ito, Y.: Challenges in unstructured mesh generation for practical and efficient computational fluid dynamics simulations. Comput Fluids 85(1):47–52 (2013).
26. Marks, A., Whidborne, J. F., Yamamoto, I.: Control allocation for fault tolerant control of a VTOL octorotor. In Proceedings of 2012 UKACC International Conference on Control pp. 357-362. IEEE, (2012)
27. Gomi, R., Takii, A., Yamakawa, M., Asao, S., Takeuchi, S., Nishimura, M.: Flight simulation from takeoff to yawing of eVTOL airplane with coaxial propellers by fluid-rigid body interaction. Advances in Aerodynamics, 5(1), 1-15 (2023).

ICCS Camera Ready Version 2023
To cite this paper please use the final published version:
DOI: 10.1007/978-3-031-35995-8_40